Research Trends and Future Perspectives on Zn-Ion Batteries Using Ga-Based Liquid Metal Coatings on Zn Anodes

ACS Energy LETTERS

http://pubs.acs.org/journal/aelccp

REVIEW

Research Trends and Future Perspectives on Zn-Ion Batteries Using Ga-Based Liquid Metal Coatings on Zn Anodes

Seungwoo Hong, Zungsun Choi, Byungil Hwang,* and Aleksandar Matic*

Cite This: *ACS Energy Lett.* 2024, 9, 5421−5433

Read Online

ACCESS | Metrics & More | Article Recommendations

ABSTRACT: **Zn-ion batteries (ZIBs) are considered promising alternatives to conventional Li-ion secondary batteries due to their high safety, environmental friendliness, and cost-effectiveness. Despite these advantages, uneven metal plating and stripping, dendrite formation, and passivation and corrosion owing to the hydrogen evolution reaction (HER) have hindered the practical implementation of ZIBs. A promising route for overcoming these problems involves coating the Zn anode with eutectic gallium indium (EGaIn)-based liquid metal (LM) with a strong Zn affinity and growth direction tenability. Despite considerable research on EGaIn-coated Zn anodes for ZIBs, this topic has not been comprehensively reviewed. Hence, this Review introduces the application of LMs to ZIBs and particularly discusses the mitigation of stability issues using LM and the fundamental processes related to Zn anodes. We summarize the progress in this field and suggest promising future research directions to advance ZIBs.**

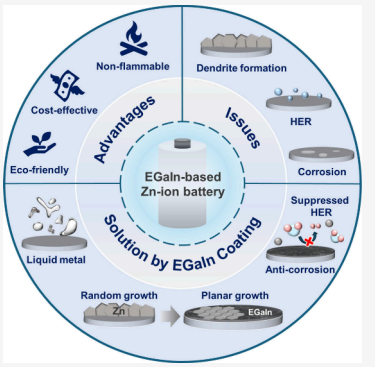

Recently, significant research efforts have been dedicated toward Zn-ion batteries (ZIBs) due to their compatibility with inexpensive, environmentally friendly, and safe aqueous-based electrolytes, higher stability than Li-ion batteries (LIBs), favorable redox potential (−0.76 V vs standard hydrogen electrode (SHE)), and high theoretical gravimetric capacity (820 mA h g^{-1}) of the Zn anode.[1,2] Due to these advantages, the applications of ZIBs are gaining traction. Nevertheless, key challenges, including uneven plating and stripping, dendrite growth, formation of side products by corrosion, such as Zn hydroxides or zincates, and surface passivation, such as by the formation of ZnO, must be addressed before the practical application and commercialization of this technology.[3−5]

Diverse research directions have been pursued to overcome these challenges. Figure 1 illustrates the timeline of the development of protective layers on Zn anodes. The majority of research efforts have been focused on various coatings on the Zn anode and achieved partial success. Specifically, organic coatings, e.g., Zn anodes coated with a carbon skeleton[6] and metal−organic frameworks (MOFs),[5,7] ensure highly uniform Zn deposition via constrained 2D surface ion migration, partly inhibiting dendrite formation. Although such attempts have improved the stabilities and performances of ZIBs, the fast-charging performances of organic coatings are limited due to low ionic conductivity and merely delay dendrite formation rather than complete prevention.[8] Hence, a strategy for effectively inhibiting dendrite formation and corrosion while ensuring sufficient rate capability, particularly during charging, continues to be critical for ZIBs.

Recently, researchers particularly emphasized the use of liquid metal (LM) electrodes to enhance battery performance.[8,10−12] LM electrodes form a unique liquid-to-liquid interface between the electrode and electrolyte, which can significantly enhance the charging performance by reducing the voltage inefficiencies stemming from various losses, including charge, ohmic, and mass transport losses. In addition, LMs exhibit no significant deformation even after large number of charge/discharge cycles, supporting improved durability.[13−16] These properties make LM anodes strong candidates for next-generation batteries.

However, the intrinsic limited structural stability of liquid electrodes, with a risk of short circuits, makes LM electrodes unsuitable in practice, particularly for wearable and flexible devices in which external stress from human motion is common.[17,18] Several attempts have been made to overcome this challenge by combining a LM with a solid ZIB electrode as a

Received: August 10, 2024
Revised: September 25, 2024
Accepted: October 7, 2024

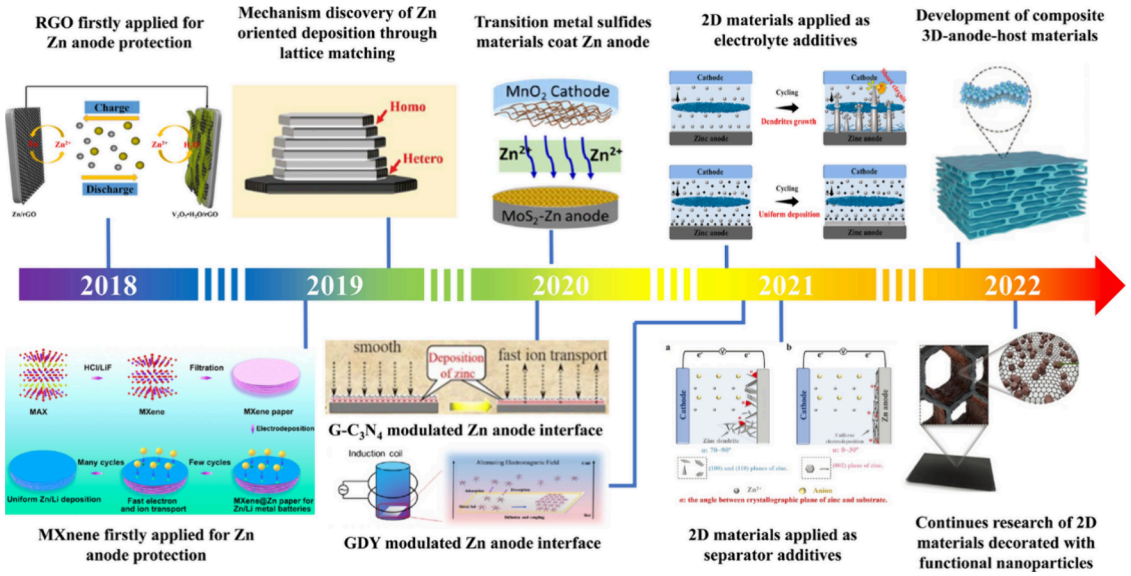

Figure 1. Timeline summarizing the development of Zn anodes and protective layers for ZIBs. Reprinted with permission from ref 9. Copyright 2023, Springer.

functional coating. Possible LMs include eutectic GaIn (EGaIn),[19] NaK,[20] eutectic GaSn (EGaSn),[21] NaZn,[22] and SbPb,[23] Among these, the EGaIn-based LM is the most promising candidate for use in ZIBs due to its strong Zn affinity, growth direction tenability, and high ionic conductivity.[10,11] In addition, the liquid state of the metal allows it to flow and fill gaps or cracks, thereby imparting self-healing properties to the LM.[24] The lack of structural stability is addressed by coating EGaIn on a solid Zn anode, thereby utilizing the excellent performance of liquid metal batteries (LMBs) without compromising structural stability.

The reduced performance of conventional Zn-ion batteries due to dendrite formation and corrosion can be greatly improved by using the eutectic gallium indium-coated Zn anode.

The reduced performance of conventional ZIBs due to dendrite formation and corrosion can be greatly improved by using the EGaIn-coated Zn anode. The primary cause of dendrite formation is the uneven charge density at the nucleated Zn sites on the surface of the solid Zn anode.[3,4] The strong Zn affinity and low Zn-ion migration energy barrier of EGaIn results in a homogeneous interfacial Zn^{2+} flux, alleviating Zn-ion depletion and inhibiting dendrite formation during charging.[13] More importantly, the alloying of Ga and In induces a change in the preferential growth direction of Zn from (100) to (002).[12] The deposition on a bare Zn anode is schematically shown in Figure 2. Figure 2a illustrates that Zn growth on the anode includes both reduction and deposition, and typically, these two steps occur simultaneously in both time and space. This results in slow redox kinetics with random growth along the (100) and (101) directions. In contrast, Zn grows preferentially along the (002) plane on the EGaIn-coated Zn anode, as shown in Figure 2b. Due to the low Zn solubility (approximately 3.0 wt% at room temperature), the reduction and deposition steps are separated in time. The reduced Zn initially dissolves into the LM interlayer

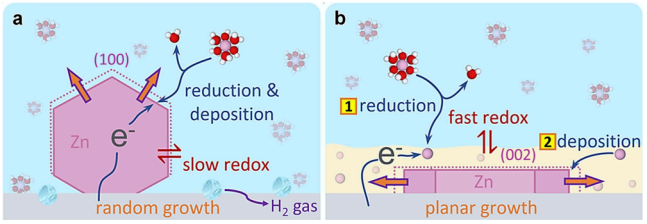

Figure 2. Schematic illustrations of Zn deposition on (a) a bare Zn anode and (b) a LM-coated anode. The pink spheres represent a Zn atom, which is surrounded by water molecules in an aqueous electrolyte; the pink solid area represents freshly deposited Zn; the gray surface represents the Zn anodes; and the yellow area in (b) represents the LM coating. Reprinted with permission from ref 12. Copyright 2023, Elsevier.

(Zn_L) and only crystallizes to Zn-anode (Zn_C) after the layer becomes saturated. In other words, the formation of crystalline Zn is delayed. This occurs since the energy required to convert Zn^{2+} to Zn_L is lower than the energy needed to transform Zn^{2+} to Zn_C. As a result, the EGaIn-coated Zn anode with a liquid−liquid interface exhibits faster redox kinetics. More importantly, the delayed formation of crystalline Zn is limited to the thin LM layer, which promotes more controlled and planar Zn growth with exposed (002) crystal planes. In addition, the deformability, self-healing properties, and high ionic conductivity of EGaIn further enhance stability during cycling and enable a high charge/discharge performance of the ZIB.[16,25]

Another feature of EGaIn-coated Zn anodes is that they can mitigate corrosion and undesirable passivation caused by the hydrogen evolution reaction (HER). In conventional ZIBs, the equilibrium potential of Zn^{2+}/Zn (−0.76 V vs SHE) is lower than that of H_2O/H_2 (0 V vs SHE), which makes the coexistence of Zn and H_2O thermodynamically unstable. This leads to spontaneous reactions in the aqueous electrolyte, releasing a H_2 gas. This, in turn, depletes the number of protons (H^+) near the electrolyte−electrode interface and creates a local alkaline environment, forming corrosive byproducts and surface passivation layers. EGaIn-coated Zn can increase the HER overpotential at the anode, as Ga (Ga^{3+}/Ga (−0.53 V vs SHE))

https://doi.org/10.1021/acsenergylett.4c02191
ACS Energy Lett. 2024, 9, 5421−5433

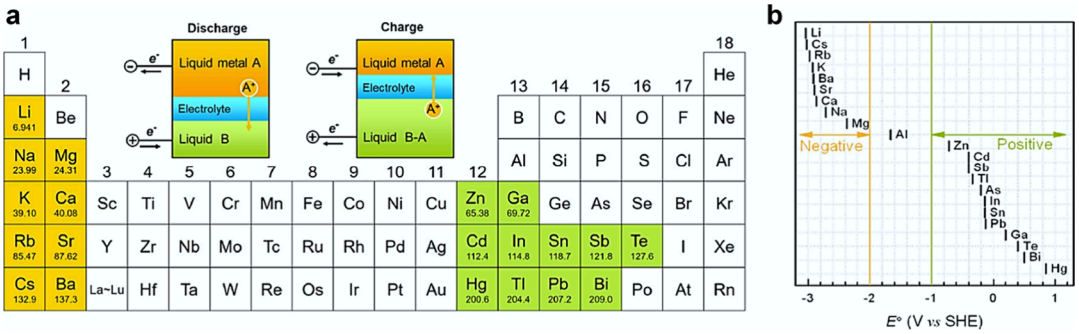

Figure 3. (a) Candidate metals for use as anode (orange) and cathode (green), along with schematic diagrams showing the discharge and charge processes. (b) Plot of the deposition potentials of candidate electrode species vs the standard hydrogen electrode (SHE) in aqueous electrolytes. Reprinted with permission from ref 27. Copyright 2023, Elsevier.

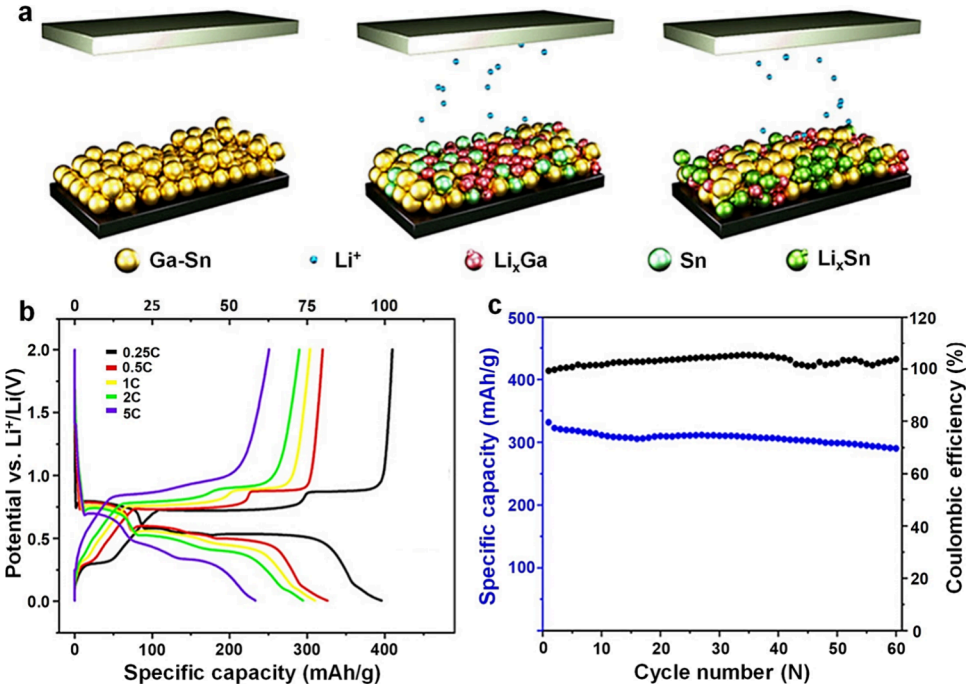

Figure 4. (a) Schematic of the electrochemical reaction mechanism of a Ga-Sn alloy electrode. Performance characteristics of an Li|Ga-Sn cell: (b) rate capability between 0.25 and 5 C and (c) cycling stability at 1 C. Reprinted with permission from ref 29. Copyright 2021, John Wiley and Sons.

and In (In^{3+}/In (−0.34 V vs SHE)) have higher overpotential than Zn for this reaction.[10,14]

In view of the increasing interest in the use of EGaIn for ZIB, the present Review is aimed at exploring the basic concepts and potential future directions related to EGaIn-coated Zn anodes. The main focus is on providing a summary and analysis of promising research avenues, the current limitations of EGaIn-based ZIBs, and proposed potential solutions for future enhancements to this technology.

THEORETICAL CLASSIFICATION OF LIQUID METALS AND LIQUID METAL BATTERIES

For use as a battery electrode, a LM must satisfy the following two criteria: (i) the melting point of the LM should be lower than 1000 °C under normal pressure. (ii) The electrical conductivity of the LM electrode must be higher than the ionic conductivities of typical electrolytes. If the electronic conductivity of the electrode is lower than these ionic conductivities, a bottleneck will be created in the deposition process, leading to inefficiencies and potential performance losses.[17,26] Figure 3a highlights materials that meet these, with the cathode candidates colored green and the anode candidates orange. Figure 3b illustrates that the highlighted materials can be categorized based on their deposition potential. Materials with deposition potentials below −2.0 V (A-type metals) can be used as the anode, while those with potentials above −1.0 V (B-type metals) are suitable for the cathode. By contrast, materials with potentials between −2.0 and −1.0 V, such as Al, do not satisfy these criteria and are therefore unsuitable for use as battery electrodes.

LMBs using single liquid phase LM electrodes operate based on the following principles. During discharge, the negative A-type metal undergoes electrochemical oxidation ($A \rightarrow A^{z+} + ze^{-1}$), thereby decreasing the thickness of the anode. The released electrons pass through the external circuit, whereas the cations travel through the electrolyte to reach the cathode (B-type), at which point they are reduced ($A^{z+} + ze^{-1} \rightarrow A$) to form

https://doi.org/10.1021/acsenergylett.4c02191
ACS Energy Lett. 2024, 9, 5421−5433

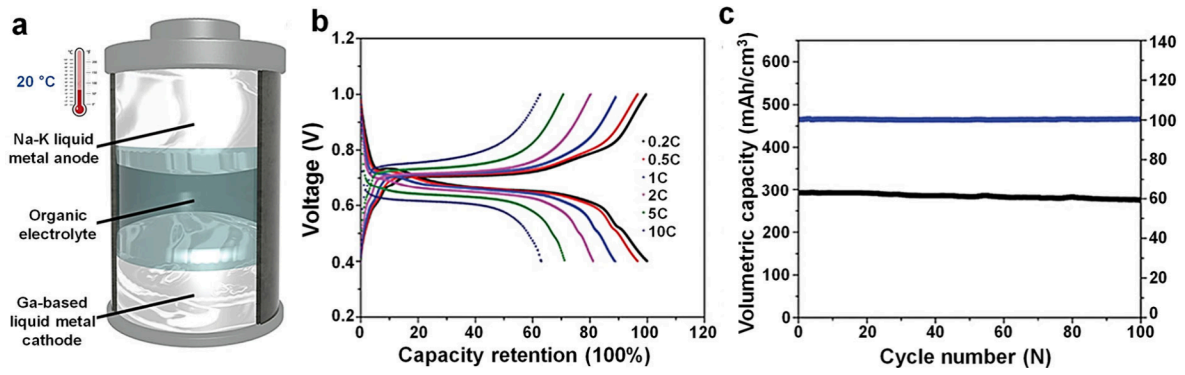

Figure 5. (a) Schematic of the three-layer liquid system in a room-temperature liquid metal battery (LMB). (b) Rate capability and (c) cycling stability of Ga-In||Na-K LMB at 1 C in an organic Na electrolyte. Reprinted with permission from ref 31. Copyright 2020, John Wiley and Sons.

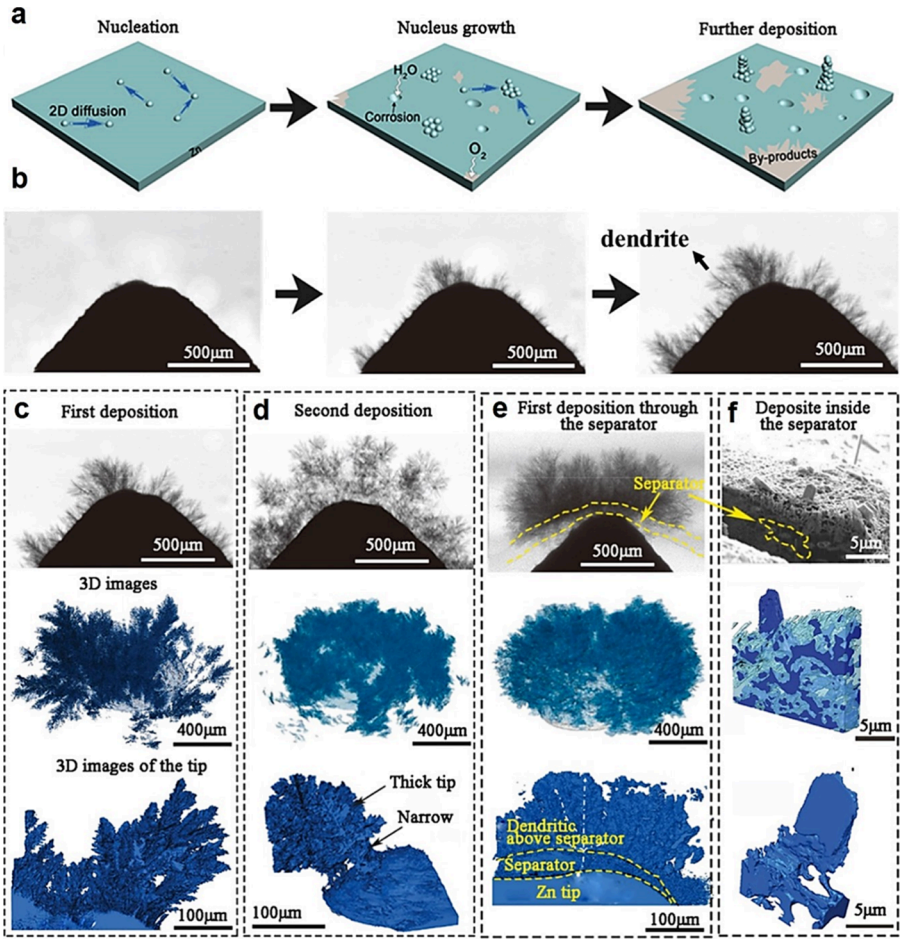

Figure 6. (a) Schematic of the growth process of Zn dendrites. (b) Operando study of the Zn dendrites in the initial growth stages. (c–e) 2D SXCT and reconstructed 3D images of Zn dendrites at the initial growth stage (c), regrowth stage after dissolution (d), and first deposition stage after perforating the porous separator (e) at a current density of 30 mA cm^{-2}. (f) Cross-sectional SEM image and reconstructed 3D images of the Zn dendrites formed at 30 mA cm^{-2}, along with the porous separator. Reproduced with permission from ref 32. Copyright 2021, Elsevier.

an A-B alloy, thereby increasing the thickness of the anode. This process is exactly reversed during charging.

Based on their working temperatures, LMBs can be classified as high-temperature LMBs (HTLMBs, >400 °C), intermediate-temperature LMBs (ITLMBs, 40–400 °C), and room-temperature LMBs (RTLMBs, 0–40 °C). Among these, RTLMBs are the most promising due to their low melting points, low potential, and high energy storage capacities. Examples of LMs with melting points below room temperature include elemental metals such as Hg, Fr, and Cs and alloys such as EGaIn, Ga-Sn, and Na-K. Hg is the least expensive but is challenging to use due to its toxicity and high vapor pressure, whereas Cs and Fr are expensive and present radiation hazards. Therefore, the current LMB research is primarily focused on the use of Ga-based alloys as electrodes.[15,28]

https://doi.org/10.1021/acsenergylett.4c02191
ACS Energy Lett. 2024, 9, 5421–5433

RECENT LITERATURE ON Ga-BASED LMBs AND THEIR LIMITATIONS

Wang et al.[29] reported cells consisting of Ga-Sn alloy cathodes and Li-metal anodes (Li||Ga-Sn). The electrochemical reaction mechanism in this system, which involves the interaction between lithium and the Ga-Sn alloy, is shown in Figure 4a. As lithium is inserted into the Ga-Sn alloy during discharge, it reacts with both gallium and tin, forming new compounds. During charge, lithium is extracted, reversing the reactions and restoring the alloy. The electrochemical performance of the cell demonstrated outstanding rate capability and high energy efficiency due to rapid charge transfer kinetics at the electrode−electrolyte interface. As shown in Figure 4b, the Li||Ga-Sn battery exhibited excellent specific capacity retention at charging rates between 0.25 and 5 C, along with 98% retention of the theoretical capacity at 0.25 C and 56% retention at 5 C. In addition, the Li||Ga-Sn cell exhibited a reliable cycling performance for 60 cycles at 1 C (Figure 4c), with a capacity retention of 87.5%, and Coulombic and energy efficiencies of 100% and 85%, respectively. The high stability of the Li||Ga-Sn cell was attributed to the self-healing property of the Ga-based alloy and the suppression of dendrite formation.

In the study by Ding et al.,[30] both electrodes were based on LMs, forming a three-layer liquid system, where Na-K, EGaIn, and a mixture of dimethoxyethane (DME) and fluoroethylene carbonate (FEC) are used as the anode, the cathode, and the electrolyte, respectively (Figure 5a). These three components naturally self-segregate due to immiscibility and density differences, preventing them from mixing. Such a unique system that forms a liquid−liquid contact significantly improves the interfacial charge transfer kinetics. As shown in Figure 5b, owing to the 3-liquid layer system, LMBs exhibited excellent capacity retention at rates up to 10 and Coulombic efficiency close to 100% even after 100 cycles (Figure 5c). These results show that LMBs have significantly improved rate performance and energy efficiency, which is necessary for an effective large-scale energy storage battery.

Although these studies have demonstrated the advantages of LMBs in terms of long-term cycling stability, high rate capability, dendrite-free characteristics, and self-healing properties, challenges due to the structural instability of the liquid electrode still remain. Liquid-based electrodes are unstable under deformation. The structural instability of an electrode can increase the risk of short circuits due to external mechanical stress, thereby limiting the application of the electrode in configurations requiring a flexible battery or a battery experiencing harsh environmental and mechanical damages.

ISSUES OCCURRING ON THE Zn ANODE IN CONVENTIONAL ZIBs

Dendrite Growth. The two key issues that occur during the anode reaction in ZIBs are dendrite growth and corrosion and passivation via the HER. Dendrite formation is caused by the nonuniform deposition of Zn due to the uneven (rough) surface of the Zn anode or ion depletion, and dendrite growth proceeds in several stages during the charging process. As schematically shown in Figure 6a, Zn dendrite growth includes a series of steps, such as Zn nucleation, nucleus growth, and further deposition. First, due to the tip effect on the rough anode surface, areas with high curvature generate strong local electric fields and higher charge densities than other regions. This increases the Zn concentration in these areas. Subsequent nucleation to deposit Zn^{2+}-ions at these sites occurs in order to lower the surface energy. As this process continues, the difference between the regions is further increased, thus resulting in the formation of dendrites. This phenomenon was visually observed by synchrotron X-ray computed tomography (SXCT), where approximately 30 μm pointed structures were observed at the initial stages of Zn growth, and as the deposition progressed, the dendrites grew longer and thicker (Figure 6b). The formation of such pointed and fragile structures can lead to capacity fading due to the creation of "dead" (inactive) Zn and decreased Coulombic efficiency. However, the most critical issue is the dendrite penetration through the separator, causing a short circuit in the cell. 2D SXCT and reconstructed 3D images of Zn dendrites at the initial growth stage clearly showed that the uneven growth of Zn at the electrode surface (Figure 6c) become denser due to reattachment from collapsed ones (Figure 6d). Consequently, the growing Zn dendrites are observed to pierce the separator and expand over the entire electrode surface (Figure 6e), causing the porous membrane to tear and short-circuit in the cell (Figure 6f).

Hydrogen Evolution Reaction. Furthermore, the HER should be reduced, as it accelerates the corrosion and passivation of the electrode. Figure 7a presents in situ optical microscopic images showing the time-lapse occurrence of the HER. A Zn anode was immersed in a 0.5 M Lithium bis(trifluoromethanesulfonyl)imide (LiTFSI) + 0.5 M zinc bis(trifluoromethanesulfonyl)imide ($Zn(TFSI)_2$) electrolyte and left standing for 5 min without applying an external potential. H_2 bubbles rapidly formed at the Zn surface, which will interfere with Zn deposition.[4,33] The HER occurs during the electrodeposition of Zn at the anode (charging), whereby the electrons transported via an external circuit simultaneously reduce the H^+

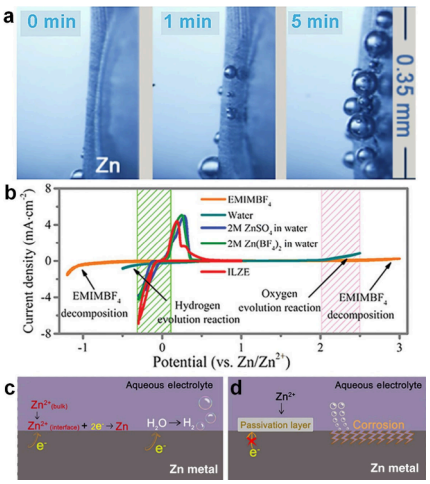

Figure 7. (a) In situ optical microscopy images of the electrolyte−Zn interface showing bubble formation due to the parasitic HER on a Zn anode at 0.2 mA cm^{-2}. Reproduced with permission from ref 38. Copyright 2022, John Wiley and Sons. (b) Electrochemical stability window of water and the ionic liquid, EMIMBF4; CV curves of Zn plating/stripping using a three-electrode configuration (stainless steel foil as a working electrode and Zn anode as reference and counter electrodes). Reproduced with permission from ref 39. Copyright 2020, John Wiley and Sons. (c, d) Schematic diagrams illustrating the (c) corrosion reaction and HER at the Zn anode surface in an aqueous electrolyte and (d) unfavorable effects at the electrolyte−Zn anode interface. Reproduced with permission from ref 38. Copyright 2022, John Wiley and Sons.

https://doi.org/10.1021/acsenergylett.4c02191
ACS Energy Lett. 2024, 9, 5421−5433

and Zn^{2+}-ions. When the battery is not operating, species such as protons or O_2 within the electrolyte act as electron acceptors and dissolve Zn, leading to the loss of active material.[1] The reaction originates from the different redox potentials of the Zn anode and the aqueous electrolyte, and in a typical electrolyte, the reaction can be represented as follows:[34]

$$2H_2O + 2e^- \leftrightarrow H_2 + 2OH^-; \quad \pm 0.83 \text{ V vs SHE} \tag{1}$$

$$ZnO + 2e^- + H_2O \leftrightarrow Zn + 2OH^-; \quad \pm 1.26 \text{ V vs SHE} \tag{2}$$

The corrosion mechanism of the Zn anode by the HER can be expressed using eqs 3, 4, and 5.[35,36]

Zn deposition:

$$Zn^{2+} + 2e^- \rightarrow Zn; \quad -0.76 \text{ V} \tag{3}$$

HER:

$$2H^+ + 2e^- \rightarrow H_2 \uparrow; \quad 0 \text{ V} \tag{4}$$

Side reaction:

$$3Zn^{2+} + 6OH^- + ZnSO_4 + xH_2O \rightarrow ZnSO_4Zn(OH)_{23}\cdot xH_2O \tag{5}$$

The reduction overpotential of the HER on the Zn anode is higher, i.e., −0.83 V, than the standard reduction potential of Zn/ZnO. Therefore, thermodynamically, the HER (eq 1) tends to occur before the reduction of ZnO (eq 2). The HER occurs when the voltage exceeds the electrochemical stability window, which depends on the pH of the electrolyte and the electric potential of the anode material, as shown in Figure 7b. Therefore, having a wide electrochemical window is important. The HER leads to the accumulation of OH^- ions near the electrode, thereby increasing the local pH and accelerating the corrosion of the electrode. Additionally, the H_2 gas generated during the HER increases internal pressure, and the HER consumes electrons from the Zn anode during charging, thereby decreasing Coulombic efficiency. These factors lead to the incomplete charging of the Zn battery, which can increase the risk of cell damage.[37]

In addition, the byproducts of the HER corrosion, such as $ZnSO_4Zn(OH)_{23}\cdot xH_2O$, lead to Zn-ion consumption in the electrolyte. The formation of byproducts consumes active Zn-ions and electrolyte, contributing to capacity fading over time (Figure 7c). Additionally, nonfaradaic reactions such as corrosion and passivation further deplete the electrolyte and reduce Zn utilization, which not only accelerates capacity loss but also shortens the overall shelf life and limits the number of charge/discharge cycles (Figure 7d). These byproducts also create nonideal surfaces on the anode, accelerate dendrite growth, increase impedance, decrease the transport rates of ions and electrons, and yield a poor Coulombic efficiency and a low energy conversion efficiency in the ZIB.[36] Such passivation and corrosion are unavoidable in ZIBs that use aqueous electrolytes. Therefore, the pH of the electrolyte must be optimized, or the HER overpotential must be increased to overcome these issues while minimizing Zn dissolution.

STRATEGIES TOWARD LONG-LIFESPAN Zn ANODES BASED ON EGaIn-BASED LMs

Coating EGaIn on a Zn anode has shown potential to resolve the limitations of LMBs and ZIBs. As Ga has high zincophilicity, EGaIn shows good wetting of Zn and provides sufficient zincophilic sites, thereby decreasing the local charge aggregation. Among the various Ga-based LMs, EGaIn is the most promising due to the high electrical conductivity of In and is more mechanically robust than the single-liquid-phase EGaIn-coated Zn anode. Pu et al.[40] performed finite element (FE) simulations of the electrochemical deposition of Zn^{2+} on Zn fibers with and without EGaIn coating. The results obtained are presented in Figure 8. A significant localization of Zn-ions

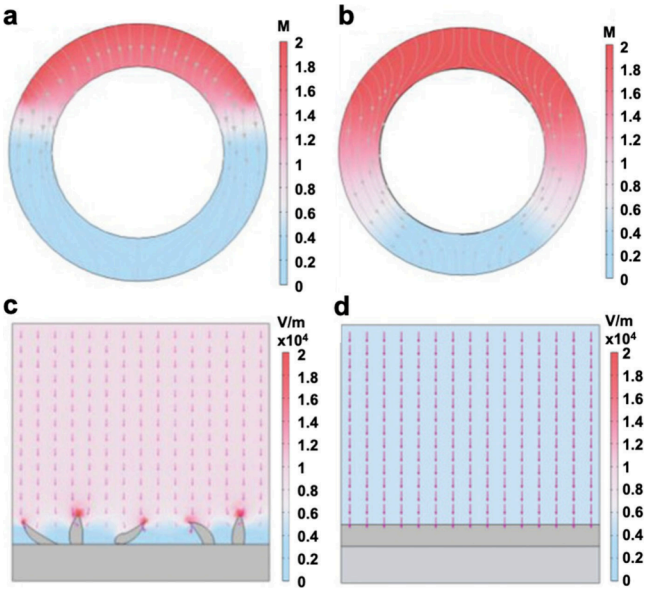

Figure 8. (a, b) FE simulations showing Zn-ion concentration distribution during Zn deposition on (a) a conventional Zn fiber, where localized Zn deposition occurs, and (b) an EGaIn-coated Zn fiber, showing more uniform Zn deposition. (c, d) Models of the electric field distribution after Zn nucleation on (c) a conventional Zn fiber, where the localized electric field accelerates dendrite formation, and (d) an EGaIn-coated Zn fiber, where the uniform electric field distribution helps prevent dendrite growth, ensuring more stable and controlled deposition. Reproduced with permission from ref 40. Copyright 2023, John Wiley and Sons.

perpendicular to the interface between the two electrodes is observed during Zn deposition (Figure 8a). As a result, Zn primarily deposits along the vertical axis, promoting dendrite growth. On the other hand, the high zincophilicity and low ion migration energy barrier of EGaIn allow Zn-ions to more easily reach the opposite end of the fiber electrode (Figure 8b). This prevents localization of Zn-ions and ensures a uniform Zn-ion concentration. In terms of the electric field (Figure 8c), the uneven deposition of Zn creates a nonuniform electric field. This leads to localized regions of high charge near the Zn nuclei, further promoting the formation of dendrites. In contrast, the LM fiber, with its uniformly distributed Zn nuclei, results in a more even electric field (Figure 8d), preventing the tipping effect seen in conventional Zn fibers and leading to a more consistent and controlled Zn deposition.

Additionally, the EGaIn coating alters the direction of crystal growth of Zn from the (100) direction (vertical) to the (002)

https://doi.org/10.1021/acsenergylett.4c02191
ACS Energy Lett. 2024, 9, 5421−5433

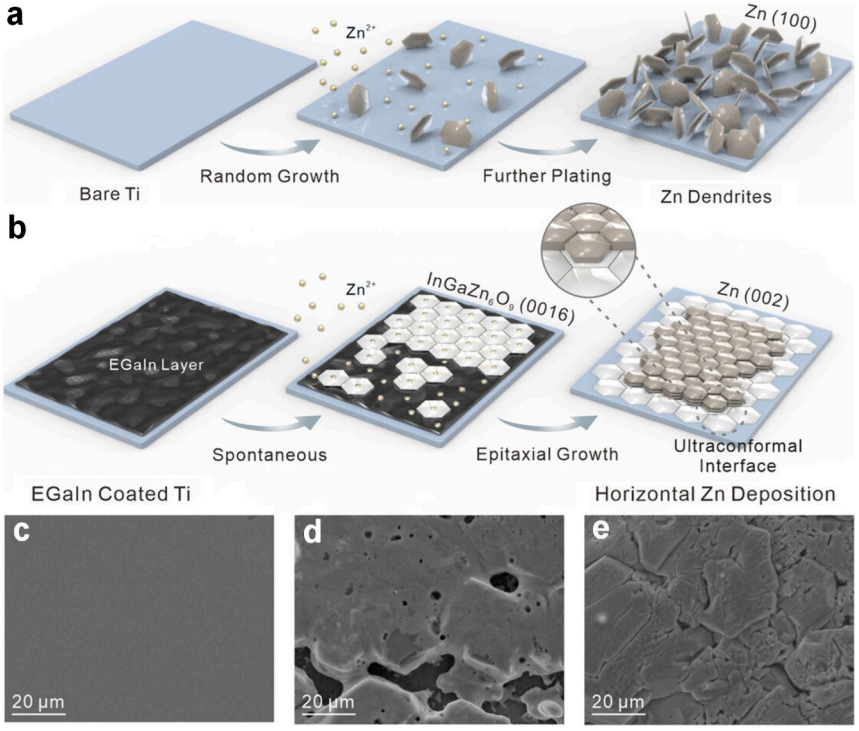

Figure 9. (a, b) Schematic diagrams of (a) dendrite formation on a bare Ti anode and (b) the suppression of dendrite formation on an $InGaZn_6O_9$@Ti anode. (c–e) SEM images of EGaIn before (c) and after the predeposition of Zn at (d) 3 mA h cm^{-2} and (e) 5 mA h cm^{-2}. Reproduced with permission from ref 41. Copyright 2020, John Wiley and Sons.

direction (horizontal), as shown schematically in Figure 9. The growth of Zn in the (100) direction forms randomly distributed columnar dendrites (Figure 9a), whereas growth along the (002) direction generates planar Zn plates without dendrite formation (Figure 9b). In the latter case, the reaction of EGaIn with Zn allows Zn to be deposited in the horizontal direction, which provides hexagonal crystal nuclei and facilitates the formation of an $InGaZn_6O_9$ alloy layer matching the (0016) plane. This indicates that EGaIn coating enables uniform and controlled deposition of Zn, thereby avoiding dendrite growth. The EGaIn coating created a smooth, flat surface across the Zn anode, as shown in Figure 9c. During the predeposition at a capacity of 3 mAh cm^{-2}, a Zn layer was grown in-plane, thereby forming a hexagonal layered structure (Figure 9d). The hexagonal Zn regions gradually stitch together as the deposition progresses, and smoother and more compact Zn deposition occurred across the electrode at higher current density (Figure 9e). In conclusion, as the reaction continues, Zn is spontaneously deposited on the $InGaZn_6O_9$ alloy along the (002) direction to create an epitaxial-like interface, enabling the creation of a stable, dendrite-free anode.

RECENT TRENDS IN EGaIn-COATED Zn ANODE BATTERIES

Several different types of EGaIn-based LMs have been applied to Zn anodes to improve the stabilities of the ZIBs. In the study conducted by Kidanu et al.,[16] EGaIn bulk liquid metal (BLM) and EGaIn/metal nanoparticles (LMNPs) were coated on Zn anode surfaces to obtain Zn@BLM and Zn@LMNP electrodes. In each case, Ga and In were mixed in a ratio of 74.5:24.5. The typical growth of Zn dendrites on the bare Zn substrate during electrochemical deposition/stripping is shown schematically in Figure 10a, whereas the nondendritic deposition of Zn on the EGaIn-coated Zn anode is shown in Figure 10b. The Zn@BLM electrode showed an even distribution of bulk liquid metal across the surface (Figure 10c), while the Zn@LMNP electrode showed relatively poor uniformity due to the clustering of nanoparticles (Figure 10d). The electrochemical performances of full cells, composed of a V_2O_5 cathode, a 2 M $ZnSO_4$ electrolyte, bare Zn, and Zn@BLM or Zn@LMNP anodes, are demonstrated in Figure 10e–f. As shown in Figure 10e, the LM coating enhanced the discharge capacity of the full cell. In addition, the cycling performance improved significantly. The bare Zn and Zn@LMNP cells short-circuit or exhibit voltage fluctuations before reaching 200 cycles, whereas Zn@BLM exhibits stable cycling even after 1000 cycles (Figure 10f).

Pu et al.[40] conducted electrochemical tests to evaluate the effectiveness of EGaIn in resisting side reactions such as corrosion and HER. This is confirmed by the Tafel plots and linear sweep voltammetry (LSV) profiles as shown in Figure 11. The EGaIn-coated Zn fiber exhibited a higher corrosion resistance potential compared to that of the bare Zn, indicating a lower tendency for corrosion (Figure 11a). The LSV results show that the EGaIn-coated Zn anode requires an overpotential of −2.1 V to reach a current density of −150 mA cm^{-2}, while the bare Zn fiber requires a slightly higher value of −2.0 V (Figure 11b). This indicates that hydrogen evolution is significantly suppressed on the EGaIn-coated Zn anode surface. These results show that EGaIn effectively enhances the lifetime stability of ZIBs by suppressing side reactions, which are a major issue in these systems.

Liu et al.[10] explored EGaIn-coated Zn anodes (EGaIn@Zn) to improve ZIB performance. The EGaIn was coated onto the Zn anode by using a doctor blade. Freshly deposited Zn atoms diffuse into the alloy interlayer, preferring to bond with the Ga-In alloy as illustrated in Figure 12a. When the Zn content exceeds the alloy's solubility limit, the excess Zn grows beneath

https://doi.org/10.1021/acsenergylett.4c02191
ACS Energy Lett. 2024, 9, 5421−5433

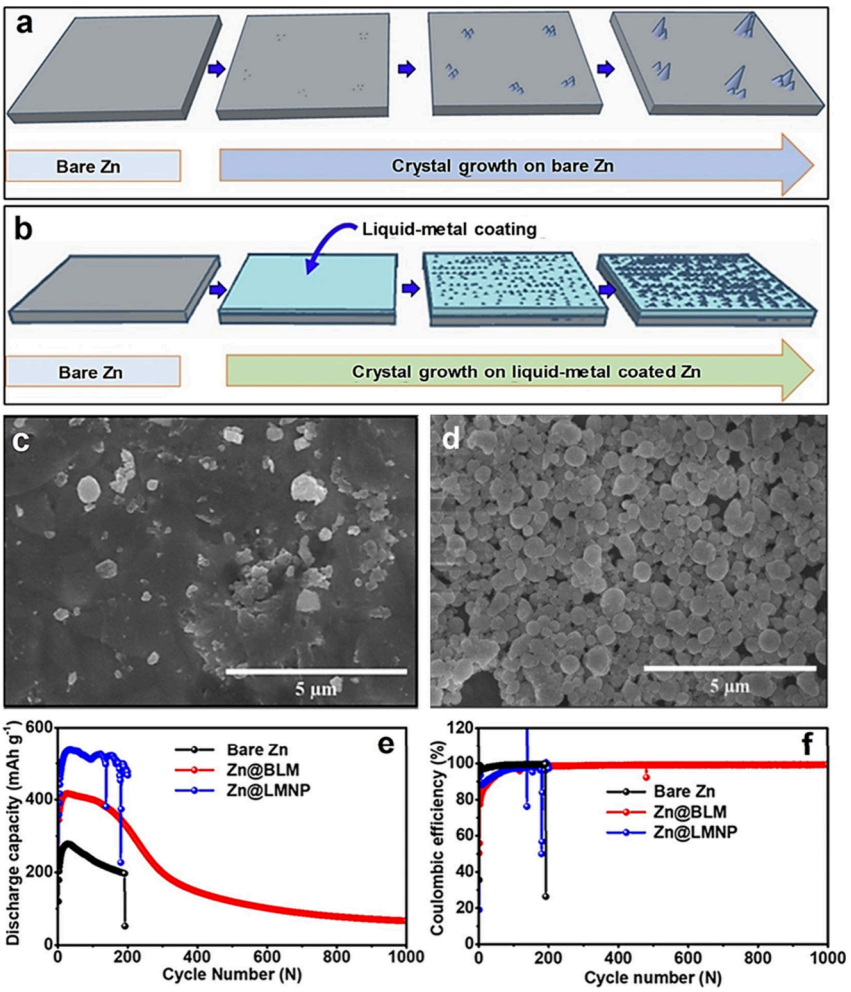

Figure 10. Schematic diagrams of Zn-ion deposition/stripping on (a) bare Zn anode and (b) bulk LM-coated substrate. (c, d) SEM images of (c) Zn@BLM and (d) Zn@LMNP electrodes. (e, f) Long-term cyclability (e) and Coulombic efficiency (f) of each cell. The electrochemical characterizations are conducted in the potential range of 0.25−1.6 V (vs Zn/Zn^{2+}) at a galvanostatic charge/discharge rate of 1 A g^{-1}. The capacities are analyzed based on the active mass of the cathode. Reproduced with permission from ref 16. Copyright 2022, MDPI.

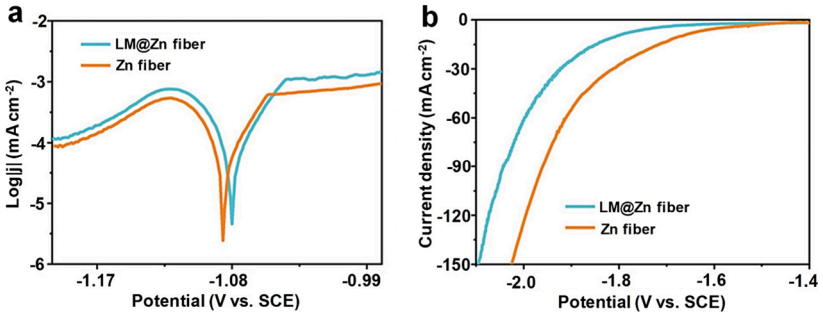

Figure 11. (a) Tafel curves of bare Zn and LM@Zn fiber anodes. (b) LSV profiles showing that the EGaIn-coated Zn anode requires a higher overpotential (−2.1 V) to reach a current density of −150 mA cm^{-2} compared with the bare Zn anode (−2.0 V). Reproduced with permission from ref 40. Copyright 2023, John Wiley and Sons.

the liquid alloy layer rather than on the surface. EGaIn coating showed no significant change in the roughness of the Zn anode, where similar height profiles of Zn anodes were observed before and after the EGaIn coating (Figure 12b). In symmetric cells, the resulting time-dependent voltage characteristics at a current density of 1 mA cm^{-2} are presented in Figure 12c. EGaIn@Zn outperforms bare Zn and operates without failure for extended periods. Full cells were constructed with either a bare Zn or EGaIn@Zn anode, an MnO_2 cathode, and 3 M $ZnSO_4$ as the electrolyte.[13] In addition, EGaIn@Zn||MnO_2 exhibits fewer fluctuations and more stable cycling compared to those of the cell with the bare Zn electrode. The EGaIn@Zn||MnO_2 ZIB also exhibited a higher capacity (Figure 12d) and smaller interfacial impedance (R_f) and charge-transfer resistance (R_{ct}) than the ZIB containing bare Zn (Figure 12e). This is related to improved charge transfer at the liquid−liquid interface of the EGaIn@Zn||MnO_2 ZIB. This suggests that undesired side reactions, such as corrosion and passivation at the interface

https://doi.org/10.1021/acsenergylett.4c02191
ACS Energy Lett. 2024, 9, 5421−5433

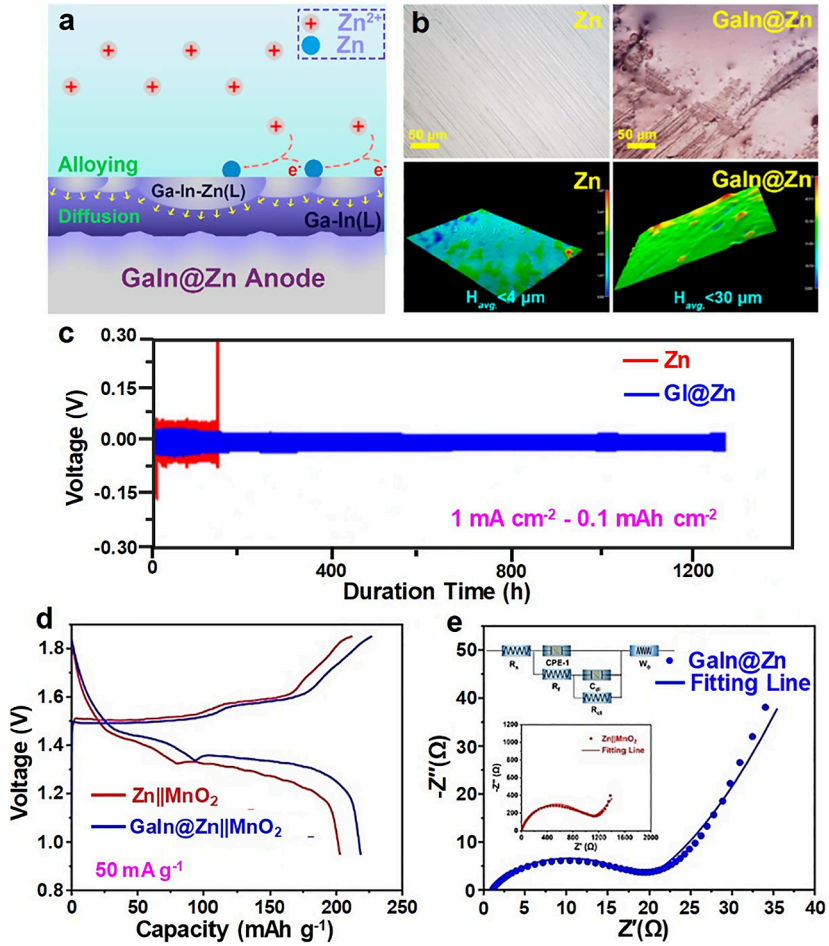

Figure 12. (a) Schematic illustration of a dendrite-free EGaIn@Zn anode fabricated via an alloying−diffusion synergistic strategy. (b) Surface optical microscopy images of freshly prepared Zn and EGaIn@Zn anodes and 3D simulation height of the Zn and EGaIn@Zn anodes. (c) Voltage profiles of symmetric Zn- and EGaIn@Zn cells at 1 mA cm^{-2} current density. (d) Typical galvanostatic charge/discharge profiles at a current density of 50 mA g^{-1}. (e) Electrochemical impedance spectroscopy measurements during the first cycle along with the fitting lines and an equivalent circuit. Reproduced with permission from ref 10. Copyright 2021, American Chemical Society.

Table 1. Techno-economic Assessment of Various Battery Systems

Material	Melting point (°C)	Potential vs SHE (V)	Ionic radius (Å)	Active ion	Earth abundance (ppm)	Cost ($/lb)	Density (g cm^{-3})	Specific gravimetric capacity	Specific volumetric capacity (mAh cm^{-3})
Li	180	−3.04	0.76	Li^+	18	8−11	0.53	3860	2061
Na	98	−2.71	1.02	Na^+	23,000	1.1−1.6	0.97	1166	1129
K	63	−2.93	1.38	K^+	21,000	3−9	0.86	687	610
Mg	651	−2.36	0.72	Mg^{2+}	23,000	1−1.5	1.74	2206	3834
Ca	842	−2.84	1.00	Ca^{2+}	41,000		1.55	1337	2072
Al	660	−1.68	0.53	Al^{3+}	82,000	0.5−1.5	2.70	2980	8046
Fe	1538	−0.45	0.78	Fe^{2+}	46,500	0.9−1	7.87	960	7558
Zn	419	−0.76	0.75	Zn^{2+}	79	1.0−1.2	7.13	820	5855
Mn	1244	−1.19	0.67	Mn^{2+}	950		7.44	976	7250
Ga	30	0.2	0.62	Ga^{3+}	16.9	129−132	5.91	769	4545
In	156	−0.18	0.8	In^{3+}	0.1	125−127	7.29	1010	

between Zn and the electrolyte due to the low HER overpotential of Zn, are limited by the EGaIn coating, thereby enhancing the stability of the ZIB.

TECHNO-ECONOMIC ASSESSMENT OF Zn-ION BATTERIES

For future large-scale energy storage systems, high electrochemical performance as well as raw material availability and cost-effectiveness are important considerations. Although LIBs are currently commercialized due to their high energy density of 240 W h kg^{-1} and long cycle life, the relatively low resource availability of Co and Ni, used in LIB cathodes, increases cost and complicates the application to large-scale energy storage systems (Table 1). ZIBs are favored as a promising alternative due to their competitive price relative to LIBs (Table 1 and Figure 13a) and the higher volumetric capacity and lower

https://doi.org/10.1021/acsenergylett.4c02191
ACS Energy Lett. 2024, 9, 5421−5433

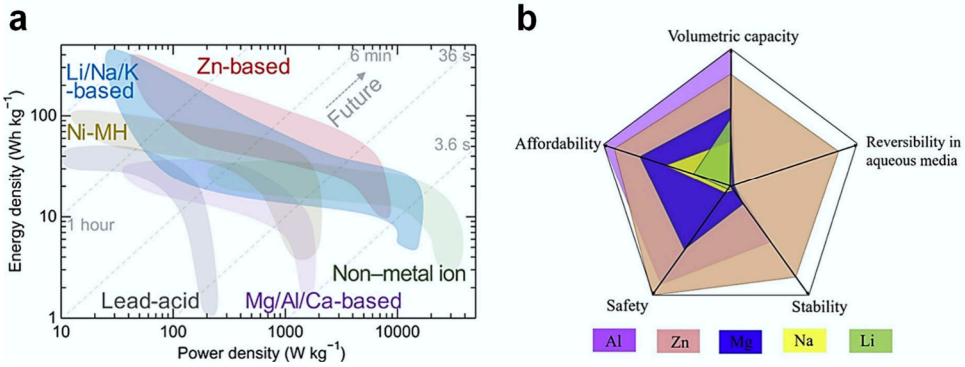

Figure 13. (a) Diagram showing the comparative property regimes of various batteries. Reproduced with permission from ref 45. Copyright 2019, Elsevier. (b) Energy density vs power density performances of some conventional commercialized batteries, including typical metal-ion batteries (Li^+, Na^+, K^+, Zn^{2+}, Mg^{2+}, Al^{2+}, and Ca^{2+}) and batteries based on non-metal-ion charge carriers. Reproduced with permission from ref 46. Copyright 2020, Science Advances.

reactivity compared to the competing alternative battery systems using K, Mg, Ca, and Na (Table 1 and Figure 13b).

> Eutectic gallium indium, which is used to address issues occurring at the anode in Zn-ion batteries, also provides environmental and safety advantages compared to conventional anode coating materials.

EGaIn, which is used to address issues occurring at the anode in ZIBs, also provides environmental and safety advantages compared to conventional anode coating materials. Commonly used anode coatings, such as MOFs and nanosheet materials,[42] are typically synthesized via hydrothermal methods or coprecipitation techniques.[43] These methods require drying or sintering at high-temperature, which possess risks of fire or explosion. In addition, the use of toxic solvents such as *N*-methyl-2-pyrrolidone (NMP) or dimethylformamide (DMF) also raises environmental and health concerns. EGaIn has low reactivity, and the maximum processing temperature is <∼180 °C. Synthesis of EGaIn uses no toxic solvents, where only the mixing of In and Ga in a proper ratio is required to make liquid EGaIn. There have also been several reports where Ga, In, and their mixture, EGaIn, are pointed out to not be harmful to life,[44] and instruments used for the human body, including melting needles, have been developed based on these materials.

In addition, although the components of EGaIn (i.e., Ga and In) are relatively expensive (Table 1), small quantities of these materials are needed for Zn anode coating; therefore, this approach retains the cost-effectiveness of the ZIBs. On average, ∼0.6 vol% of EGaIn relative to the total anode effectively addresses the issues occurring on the Zn anode.[16]

SUMMARY AND PERSPECTIVES

In this Review, the EGaIn interlayer was discussed as a potential solution to solve the stability issues arising at the anode in ZIBs. EGaIn induces Zn (002) deposition and exhibits a strong Zn affinity, thereby reducing local charge aggregation and enabling uniform Zn deposition. In addition, EGaIn has high corrosion and HER resistance due to its high overpotential. Thus, EGaIn-based ZIBs show excellent long-term cycling stability and reversibility and low-voltage hysteresis. Furthermore, the liquid−liquid interface between the electrode and electrolyte enables rapid Zn nucleation and fast electron transfer during repetitive Zn plating/stripping, thereby improving the overall cell performance.

Table 2 summarizes the recent literature on ZIBs using Zn anodes with different coating materials. Among them, ZIBs coated with EGaIn coating exhibit the best cyclic stability, i.e., ≳90% after 1000 cycles, which is attributed to the effective suppression of dendrite formation and the HER-led corrosion/passivation. Despite the successful examples of ZIBs using Zn anodes with EGaIn-based coatings, several issues must still be addressed in future research.

The currently adopted coating method of EGaIn requires further optimization for mass production. Brush-based coating is currently the most common method to coat EGaIn on a Zn anode. Such brush coating is effective to handle EGaIn with a high surface energy, but no studies have been done to develop automatic brush tools for scalable and large-area applications. It is also challenging to form uniform EGaIn coatings with an automatic brush. In addition, the high surface energy of EGaIn limits the use of conventional coating tools such as doctor blade. Thus, developing effective additives that can reduce the surface energy of EGaIn is an important research direction for EGaIn-based ZIBs. Developing surface treatment technology of the Zn anode to promote the interfacial adhesion between EGaIn and the Zn anode is a promising alternative strategy for scalable production of EGaIn-based ZIBs.

Second, the energy storage capacity and working voltage of the LM-based ZIB remains smaller than those of its competitors, including LIBs and Na-ion batteries.[13,47] As listed in Table 2, the number of studies on ZIBs using Zn anodes with EGaIn-based coatings has been limited thus far. This research is in the initial stages; therefore innovative solutions involving changing the electrolyte or cathode are needed for improving the electrochemical performance parameters. The water used as the electrolyte in ZIBs theoretically undergoes electrolysis at a voltage of 1.23 V. Although the presence of salts and an overpotential allow it to withstand slightly higher voltages, the maximum voltage typically used in experiments is still around 1.8−1.9 V. This is significantly lower compared to LIBs, which operates above 3 V, and is highly disadvantageous for energy density. Therefore, research is needed to develop electrolytes that do not decompose at higher voltages by exploring additives and alternative solvent. Additionally, screening the best cathode materials for ZIBs with Zn anodes with EGaIn-based coatings

https://doi.org/10.1021/acsenergylett.4c02191
ACS Energy Lett. 2024, 9, 5421−5433

Table 2. Comparison of Electrochemical Performances of ZIBs According to Anode Materials

Anode	Cathode	Electrolyte	Specific capacity Current density	Capacity retention (no. of cycles) Current density	Voltage range (V)	Refs
Zn@HSTF	MnO_2	1 M $ZnSO_4$ + 0.1 M $MnSO_4$	163.4 mAh g^{-1} 1000 mA g^{-1}	85% (1000) 1000 mA g^{-1}	0.8−1.8	48
Zn@GF	Prussian blue	0.5 M Na_2SO_4 + 0.5 M $ZnSO_4$	81 mAh g^{-1} 100 mA g^{-1}	85% (150) 100 mA g^{-1}	0.8−1.6	49
Zn@CNT	MnO_2	2 M $ZnSO_4$ + 0.1 M $MnSO_4$	318.5 mAh g^{-1} 0.3 A g^{-1}	65% (1000) 3.0 A g^{-1}	1.0−1.9	50
Zn@TiO_2	MnO_2 nanowire	3 M $Zn(SO_3CF_3)_2$	235 mAh g^{-1} 100 mA g^{-1}	85% (1000) 3 mA cm^{-2}	∼1.8	51
Zn@$CaCO_3$	MnO_2	3 M $ZnSO_4$ + 0.1 M $MnSO_4$	206 mAh g^{-1} 1 A g^{-1}	86% (1000) 1 A g^{-1}	0.8−1.9	52
Zn@Graphite	$V_2O_5{\cdot}xH_2O$	2 M $ZnSO_4$	106.5 mAh g^{-1} 5 A g^{-1}	84% (1500) 5 A g^{-1}	0.4−1.6	53
EGaIn-coated Zn anode Ga:In = 75:25	MnO_2	2 M $ZnSO_4$ + 0.1 M $MnSO_4$	∼200−225 mAh g^{-1} 50 mA g^{-1}	96% (1000) 1000 mA g^{-1}	0.8−1.8	54
EGaIn-coated Zn anode Ga:In = 74.5:24.5	V_2O_5	2 M $ZnSO_4$	417 mAh g^{-1}	90% (20)	0.25−1.6	16
Ga-In-Zn-coated Zn anode Ga:In:Zn = 80:10:10	MnO_2@Carbon cloth	2 M $ZnSO_4$ + 0.1 M $MnSO_4$	185 mAh g^{-1} 1 A g^{-1}	99.7% (10 000) 5 A g^{-1}	1.0−1.8	8
EGaIn-coated Zn anode Ga:In = 78.4:21.6	MnO_2	2 M $ZnSO_4$ + 0.1 M $MnSO_4$	260 mAh g^{-1} 0.5 A g^{-1}	∼100% (240) 0.5 A g^{-1}	0.8−1.9	41
EGaIn-coated Zn fiber Ga:In = 75.5:24.5	V_2O_5@Carbon fiber	2 M $ZnSO_4$	296.8 mWh cm^{-3}	92.5% (600) 2 A cm^{-3}	0.3−1.7	11
GaInSn-coated Zn anode Ga:In:Sn = 68.5:21.5:10	$(NH_4)_2V_6O_{16}{\cdot}1.5H_2O$	2 M $ZnSO_4$	280 mAh g^{-1} 0.4 A g^{-1}	∼100% (1000) 2 A g^{-1}	∼0−2	12

still requires large efforts to achieve high-performance ZIBs using EGaIn coatings.

Given the clear potential of eutectic gallium indium-based coatings for improving zinc-ion battery stability, future research efforts will likely establish EGaIn as a key game-changing material for the commercialization of ZIBs.

Third, a detailed fundamental study of overcoming the stability challenges using LM coatings is required. To date, the electrochemical behaviors of ZIBs using Zn anodes with EGaIn-based coatings have been investigated through ex situ analysis aided by FE simulations. Although this clarifies the working principles of LMs coated on Zn anodes during the charging/discharging process, the detailed mechanism related to the microstructural changes or solid electrolyte interphase and the reasons for these occurrences remain ambiguous. These can be achieved by employing various characterization analyses, including in situ structural or compositional testing supported by theoretical calculations. A more detailed analysis for the morphological dynamics, real-time phase changes, and deposition processes occurring at Zn anodes during charging/discharging will allow the development of highly efficient and stable ZIBs. Given the clear potential of eutectic gallium indium-based coatings for improving ZIB stability, future research efforts will likely establish EGaIn as a key game-changing material for the commercialization of ZIBs.

AUTHOR INFORMATION

Corresponding Authors

Byungil Hwang − *School of Integrative Engineering, Chung-Ang University, Seoul 06974, Republic of Korea;* orcid.org/0000-0001-9270-9014; Email: bihwang@cau.ac.kr

Aleksandar Matic − *Department of Physics, Chalmers University of Technology, SE412 96 Götenburg, Sweden;* orcid.org/0000-0003-4414-9504; Email: matic@chalmers.se

https://doi.org/10.1021/acsenergylett.4c02191
ACS Energy Lett. 2024, 9, 5421−5433

Authors

Seungwoo Hong − *School of Integrative Engineering, Chung-Ang University, Seoul 06974, Republic of Korea*

Zungsun Choi − *School of Engineering, Handong Global University, Pohang 37554, Republic of Korea*

Complete contact information is available at: https://pubs.acs.org/10.1021/acsenergylett.4c02191

Notes

The authors declare no competing financial interest.

Biographies

Seungwoo Hong received his Bachelor's degree from the School of Integrative Engineering from Chung-Ang University in South Korea in 2023. He is currently pursuing his M.S. degree at the same university. His research focuses on developing novel anode and cathode materials for high-performance ZIBs.

Zungsun Choi is an Associate Professor at Handong Global University. He obtained his B.Eng. degree from Cornell University and Ph.D. from the Massachusetts Institute of Technology, with postdoc trainings at Karlsruhe Institute of Technology. His research interests focus on anode/cathode materials for secondary batteries and recycling of battery materials.

Byungil Hwang is an Associate Professor in the School of Integrative Engineering at Chung-Ang University in South Korea. He is the Director of the Korea-Sweden Advanced Textile Energy Materials Innovation Center. His research focuses on the reliability of materials for energy storage/harvesting and electronics applications.

Aleksandar Matic is a Professor in the Department of Physics at Chalmers University of Technology, Sweden, and leads the Division of Materials Physics. He is also leading the strategic initiative in research and education for battery technology. His research focuses on next-generation batteries, particularly metal anodes and operando characterization.

■ ACKNOWLEDGMENTS

This research was supported by the GRDC (Global Research Development Center) Cooperative Hub Program through the National Research Foundation of Korea (NRF), funded by the Ministry of Science and ICT (MSIT) (RS-2023-00257595).

■ REFERENCES

(1) Fang, G.; Zhou, J.; Pan, A.; Liang, S. Recent advances in aqueous zinc-ion batteries. *ACS Energy Lett.* **2018**, *3* (10), 2480−2501. Ming, J.; Guo, J.; Xia, C.; Wang, W.; Alshareef, H. N. Zinc-ion batteries: Materials, mechanisms, and applications. *Mater. Sci. Eng. R Rep.* **2019**, *135*, 58−84.

(2) Zhang, T.; Tang, Y.; Guo, S.; Cao, X.; Pan, A.; Fang, G.; Zhou, J.; Liang, S. Fundamentals and perspectives in developing zinc-ion battery electrolytes: a comprehensive review. *Energy Environ. Sci.* **2020**, *13* (12), 4625−4665.

(3) Tang, B.; Shan, L.; Liang, S.; Zhou, J. Issues and opportunities facing aqueous zinc-ion batteries. *Energy Environ. Sci.* **2019**, *12* (11), 3288−3304.

(4) Xie, C.; Li, Y.; Wang, Q.; Sun, D.; Tang, Y.; Wang, H. Issues and solutions toward zinc anode in aqueous zinc-ion batteries: a mini review. *Carbon Energy* **2020**, *2* (4), 540−560.

(5) Li, C.; Xie, X.; Liang, S.; Zhou, J. Issues and future perspective on zinc metal anode for rechargeable aqueous zinc-ion batteries. *Energy Environ. Mater.* **2020**, *3* (2), 146−159.

(6) Jiang, Z.; Zhai, S.; Shui, L.; Shi, Y.; Chen, X.; Wang, G.; Chen, F. Dendrite-free Zn anode supported with 3D carbon nanofiber skeleton towards stable zinc ion batteries. *J. Colloid Interface Sci.* **2022**, *623*, 1181−1189. Xue, M.; Bai, J.; Wu, M.; He, Q.; Zhang, Q.; Chen, L. Carbon-assisted anodes and cathodes for zinc ion batteries: From basic science to specific applications, opportunities and challenges. *Energy Storage Mater.* **2023**, *62*, No. 102940.

(7) Gopalakrishnan, M.; Ganesan, S.; Nguyen, M. T.; Yonezawa, T.; Praserthdam, S.; Pornprasertsuk, R.; Kheawhom, S. Critical roles of metal−organic frameworks in improving the Zn anode in aqueous zinc-ion batteries. *Chem. Eng. J.* **2023**, *457*, No. 141334.

(8) Jia, H.; Wang, Z.; Dirican, M.; Qiu, S.; Chan, C. Y.; Fu, S.; Fei, B.; Zhang, X. A liquid metal assisted dendrite-free anode for high-performance Zn-ion batteries. *J. Mater. Chem. A* **2021**, *9* (9), 5597−5605.

(9) Zheng, S.; Zhao, W.; Chen, J.; Zhao, X.; Pan, Z.; Yang, X. 2D materials boost advanced Zn anodes: principles, advances, and challenges. *Nano-Micro Letters* **2023**, *15* (1), 46.

(10) Liu, C.; Luo, Z.; Deng, W.; Wei, W.; Chen, L.; Pan, A.; Ma, J.; Wang, C.; Zhu, L.; Xie, L.; et al. Liquid alloy interlayer for aqueous zinc-ion battery. *ACS Energy Lett.* **2021**, *6* (2), 675−683.

(11) Pu, J.; Cao, Q.; Gao, Y.; Wang, Q.; Geng, Z.; Cao, L.; Bu, F.; Yang, N.; Guan, C. Liquid Metal-Based Stable and Stretchable Zn-Ion Battery for Electronic Textiles. *Adv. Mater.* **2024**, *36* (2), No. 2305812.

(12) Chen, H.; Guo, Z.; Wang, H.; Huang, W.; Pan, F.; Wang, Z. A liquid metal interlayer for boosted charge transfer and dendrite-free deposition toward high-performance Zn anodes. *Energy Storage Mater.* **2023**, *54*, 563−569.

(13) Zou, J.; Zeng, Z.; Wang, C.; Zhu, X.; Zhang, J.; Lan, H.; Li, L.; Yu, Y.; Wang, H.; Zhu, X.; et al. Ultraconformal Horizontal Zinc Deposition toward Dendrite-Free Anode. *Small Structures* **2023**, *4* (1), No. 2200194.

(14) Wang, K.; Hu, J.; Chen, T.; Wang, K.; Wu, J.; Chen, Q.; Deng, Z.; Zhang, W. Interface Engineering of Flexible Liquid Metal Modulation To Achieve Dendrite-Free Zinc Metal Anodes. *ACS Sustain. Chem. Eng.* **2023**, *11* (24), 9111−9120.

(15) Yang, J.; Kwon, K. Y.; Kanetkar, S.; Xing, R.; Nithyanandam, P.; Li, Y.; Jung, W.; Gong, W.; Tuman, M.; Shen, Q.; et al. Skin-Inspired Capacitive Stress Sensor with Large Dynamic Range via Bilayer Liquid Metal Elastomers. *Advanced Materials Technologies* **2022**, *7* (5), No. 2101074.

(16) Kidanu, W. G.; Yang, H.; Park, S.; Hur, J.; Kim, I. T. Room-Temperature Liquid-Metal Coated Zn Electrode for Long Life Cycle Aqueous Rechargeable Zn-Ion Batteries. *Batteries* **2022**, *8* (11), 208.

(17) Kim, H.; Boysen, D. A.; Newhouse, J. M.; Spatocco, B. L.; Chung, B.; Burke, P. J.; Bradwell, D. J.; Jiang, K.; Tomaszowska, A. A.; Wang, K.; et al. Liquid metal batteries: past, present, and future. *Chem. Rev.* **2013**, *113* (3), 2075−2099.

(18) Zhang, S.; Liu, Y.; Fan, Q.; Zhang, C.; Zhou, T.; Kalantar-Zadeh, K.; Guo, Z. Liquid metal batteries for future energy storage. *Energy Environ. Sci.* **2021**, *14* (8), 4177−4202.

(19) Liu, D.; Su, L.; Liao, J.; Reeja-Jayan, B.; Majidi, C. Rechargeable Soft-Matter EGaIn-MnO2 Battery for Stretchable Electronics. *Adv. Energy Mater.* **2019**, *9* (46), No. 1902798. Yang, J.; Cao, J.; Han, J.; Xiong, Y.; Luo, L.; Dan, X.; Yang, Y.; Li, L.; Sun, J.; Sun, Q. Stretchable multifunctional self-powered systems with Cu-EGaIn liquid metal electrodes. *Nano Energy* **2022**, *101*, No. 107582.

(20) Huang, M.; Xi, B.; Feng, Z.; Wu, F.; Wei, D.; Liu, J.; Feng, J.; Qian, Y.; Xiong, S. New insights into the electrochemistry superiority of liquid Na-K alloy in metal batteries. *Small* **2019**, *15* (12), No. 1804916. Xie, Y.; Hu, J.; Zhang, Z. A stable carbon host engineering surface defects for room-temperature liquid NaK anode. *J. Electroanal. Chem.* **2020**, *856*, No. 113676.

(21) Wang, K.; Hu, J.; Chen, T.; Wang, K.; Deng, Z.; Wu, J.; Feng, Y.; Chen, Q.; Zhang, W. A yolk-shell eGaSn@ Void@ SiO2 nanodroplet design for high-performance cathodes in room temperature liquid metal batteries. *Compos. B Eng.* **2023**, *250*, No. 110423.

(22) Xu, J.; Kjos, O. S.; Osen, K. S.; Martinez, A. M.; Kongstein, O. E.; Haarberg, G. M. Na-Zn liquid metal battery. *J. Power Sources* **2016**, *332*, 274−280. Xu, J.; Martinez, A. M.; Osen, K. S.; Kjos, O. S.; Kongstein, O. E.; Haarberg, G. M. Electrode behaviors of Na-Zn liquid metal battery. *J. Electrochem. Soc.* **2017**, *164* (12), A2335.

(23) Li, X.; Qu, J.; Zhao, Z.; Zhao, Y.; Xie, H.; Yin, H. Electrochemical desulfurization of galena-stibnite in molten salts to prepare liquid Sb−Pb alloy for liquid metal battery. *J. Clean. Prod.* **2021**, *312*, No. 127779.
(24) Zhang, K. Q.; ur Rehman, K.; Gao, J. Liquid Metal-Promoted Graphene Oxide Supramolecular Film for Self-Healing Actuator with Multiple-Stimuli Responses. *Chem.—Asian J.* **2023**, *18* (14), No. e202300409.
(25) Shi, G.; Peng, X.; Zeng, J.; Zhong, L.; Sun, Y.; Yang, W.; Zhong, Y. L.; Zhu, Y.; Zou, R.; Admassie, S.; et al. A Liquid Metal Microdroplets Initialized Hemicellulose Composite for 3D Printing Anode Host in Zn-Ion Battery. *Adv. Mater.* **2023**, *35* (25), No. 2300109.
(26) Li, H.; Yin, H.; Wang, K.; Cheng, S.; Jiang, K.; Sadoway, D. R. Liquid metal electrodes for energy storage batteries. *Adv. Energy Mater.* **2016**, *6* (14), No. 1600483. Ding, Y.; Guo, X.; Yu, G. Next-generation liquid metal batteries based on the chemistry of fusible alloys. *ACS Cent. Sci.* **2020**, *6* (8), 1355−1366.
(27) Wu, S.; Zhang, X.; Wang, R.; Li, T. Progress and perspectives of liquid metal batteries. *Energy Storage Mater.* **2023**, *57*, 205−227.
(28) Agarwal, D.; Potnuru, R.; Kaushik, C.; Darla, V. R.; Kulkarni, K.; Garg, A.; Gupta, R. K.; Tiwari, N.; Nalwa, K. S. Recent advances in the modeling of fundamental processes in liquid metal batteries. *Renew. Sustain. Energy Rev.* **2022**, *158*, No. 112167. Zhang, B. W.; Ren, L.; Wang, Y. X.; Xu, X.; Du, Y.; Dou, S. X. Gallium-based liquid metals for lithium-ion batteries. *Interd. Mater.* **2022**, *1* (3), 354−372.
(29) Wang, K.; Hu, J.; Chen, T.; Tang, J.; Wang, Z.; Fan, N.; Zhang, W.; Wang, K. A High-Performance Room-Temperature Li||Ga-Sn Liquid Metal Battery for Grid Energy Storage. *Energy Technol.* **2021**, *9* (9), No. 2100330.
(30) Ding, Y.; Guo, X.; Qian, Y.; Xue, L.; Dolocan, A.; Yu, G. Room-temperature all-liquid-metal batteries based on fusible alloys with regulated interfacial chemistry and wetting. *Adv. Mater.* **2020**, *32* (30), No. 2002577.
(31) Ding, Y.; Guo, X.; Qian, Y.; Xue, L.; Dolocan, A.; Yu, G. Room-Temperature All-Liquid-Metal Batteries Based on Fusible Alloys with Regulated Interfacial Chemistry and Wetting. *Adv. Mater.* **2020**, *32* (30), No. 2002577.
(32) Zheng, X.; Ahmad, T.; Chen, W. Challenges and strategies on Zn electrodeposition for stable Zn-ion batteries. *Energy Storage Mater.* **2021**, *39*, 365−394.
(33) Du, W.; Ang, E. H.; Yang, Y.; Zhang, Y.; Ye, M.; Li, C. C. Challenges in the material and structural design of zinc anode towards high-performance aqueous zinc-ion batteries. *Energy Environ. Sci.* **2020**, *13* (10), 3330−3360.
(34) Li, Y.; Wang, Z.; Cai, Y.; Pam, M. E.; Yang, Y.; Zhang, D.; Wang, Y.; Huang, S. Designing Advanced Aqueous Zinc-Ion Batteries: Principles, Strategies, and Perspectives. *Energy Environ. Mater.* **2022**, *5* (3), 823−851. Wang, T.; Li, C.; Xie, X.; Lu, B.; He, Z.; Liang, S.; Zhou, J. Anode materials for aqueous zinc ion batteries: mechanisms, properties, and perspectives. *ACS Nano* **2020**, *14* (12), 16321−16347.
(35) Lv, Y.; Xiao, Y.; Ma, L.; Zhi, C.; Chen, S. Recent advances in electrolytes for "beyond aqueous" zinc-ion batteries. *Adv. Mater.* **2022**, *34* (4), No. 2106409. He, P.; Chen, Q.; Yan, M.; Xu, X.; Zhou, L.; Mai, L.; Nan, C.-W. Building better zinc-ion batteries: A materials perspective. *EnergyChem.* **2019**, *1* (3), No. 100022.
(36) Zhang, X.; Hu, J. P.; Fu, N.; Zhou, W. B.; Liu, B.; Deng, Q.; Wu, X. W. Comprehensive review on zinc-ion battery anode: challenges and strategies. *InfoMat* **2022**, *4* (7), No. e12306.
(37) Ma, L.; Chen, S.; Li, N.; Liu, Z.; Tang, Z.; Zapien, J. A.; Chen, S.; Fan, J.; Zhi, C. Hydrogen-free and dendrite-free all-solid-state Zn-ion batteries. *Adv. Mater.* **2020**, *32* (14), No. 1908121.
(38) Zhang, X.; Hu, J.-P.; Fu, N.; Zhou, W.-B.; Liu, B.; Deng, Q.; Wu, X.-W. Comprehensive review on zinc-ion battery anode: Challenges and strategies. *InfoMat* **2022**, *4* (7), No. e12306.
(39) Ma, L.; Chen, S.; Li, N.; Liu, Z.; Tang, Z.; Zapien, J. A.; Chen, S.; Fan, J.; Zhi, C. Hydrogen-free and dendrite-free all-solid-state Zn-ion batteries. *Adv. Mater.* **2020**, *32* (14), No. 1908121.
(40) Pu, J.; Cao, Q.; Gao, Y.; Wang, Q.; Geng, Z.; Cao, L.; Bu, F.; Yang, N.; Guan, C. Liquid Metal-Based Stable and Stretchable Zn-Ion Battery for Electronic Textiles. *Adv. Mater.* **2024**, *36* (2), No. 2305812.
(41) Zou, J.; Zeng, Z.; Wang, C.; Zhu, X.; Zhang, J.; Lan, H.; Li, L.; Yu, Y.; Wang, H.; Zhu, X.; et al. Ultraconformal Horizontal Zinc Deposition toward Dendrite-Free Anode. *Small Structures* **2023**, *4* (1), No. 2200194.
(42) Zhang, Y.; Zhu, M.; Wang, G.; Du, F. H.; Yu, F.; Wu, K.; Wu, M.; Dou, S. X.; Liu, H. K.; Wu, C. Dendrites-free Zn metal anodes enabled by an artificial protective layer filled with 2D anionic Nanosheets. *Small Methods* **2021**, *5* (10), No. 2100650. Wu, L.; Zhang, Y.; Shang, P.; Dong, Y.; Wu, Z.-S. Redistributing Zn ion flux by bifunctional graphitic carbon nitride nanosheets for dendrite-free zinc metal anodes. *Journal of Materials Chemistry A* **2021**, *9* (48), 27408−27414. Zhang, W.; Qi, W.; Yang, K.; Hu, Y.; Jiang, F.; Liu, W.; Du, L.; Yan, Z.; Sun, J. Boosting tough metal Zn anode by MOF layer for high-performance zinc-ion batteries. *Energy Storage Materials* **2024**, *71*, No. 103616.
(43) Shangguan, E.; Li, L.; Wu, C.; Ning, S.; Wang, M.; Li, L.; Zhao, L.; Li, Q.; Li, J. Comparative structural and electrochemical study of spherical ZnO with different tap density and morphology as anode materials for Ni/Zn secondary batteries. *J. Alloys Compd.* **2021**, *868*, No. 159141. Wang, C.; Wei, S.; Chen, S.; Cao, D.; Song, L. Delaminating vanadium carbides for zinc-ion storage: Hydrate precipitation and H+/Zn2+ Co-action mechanism. *Small Methods* **2019**, *3* (12), No. 1900495.
(44) Park, Y. G.; Lee, G. Y.; Jang, J.; Yun, S. M.; Kim, E.; Park, J. U. Liquid metal-based soft electronics for wearable healthcare. *Adv. Healthcare Mater.* **2021**, *10* (17), No. 2002280. Cao, J.; Li, X.; Liu, Y.; Zhu, G.; Li, R.-W. Liquid metal-based electronics for on-skin healthcare. *Biosensors* **2023**, *13* (1), 84.
(45) Li, H.; Ma, L.; Han, C.; Wang, Z.; Liu, Z.; Tang, Z.; Zhi, C. Advanced rechargeable zinc-based batteries: Recent progress and future perspectives. *Nano Energy* **2019**, *62*, 550−587.
(46) Chao, D.; Zhou, W.; Xie, F.; Ye, C.; Li, H.; Jaroniec, M.; Qiao, S.-Z. Roadmap for advanced aqueous batteries: From design of materials to applications. *Sci. Adv.* **2020**, *6* (21), No. eaba4098.
(47) Yu, P.; Zeng, Y.; Zhang, H.; Yu, M.; Tong, Y.; Lu, X. Flexible Zn-ion batteries: recent progresses and challenges. *Small* **2019**, *15* (7), No. 1804760.
(48) Xue, P.; Guo, C.; Wang, N.; Zhu, K.; Jing, S.; Kong, S.; Zhang, X.; Li, L.; Li, H.; Feng, Y.; et al. Synergistic manipulation of Zn2+ ion flux and nucleation induction effect enabled by 3D hollow SiO2/TiO2/carbon fiber for long-lifespan and dendrite-free Zn−metal composite anodes. *Adv. Funct. Mater.* **2021**, *31* (50), No. 2106417.
(49) Dong, W.; Shi, J.-L.; Wang, T.-S.; Yin, Y.-X.; Wang, C.-R.; Guo, Y.-G. 3D zinc@ carbon fiber composite framework anode for aqueous Zn−MnO 2 batteries. *RSC Adv.* **2018**, *8* (34), 19157−19163.
(50) Gao, C.; Wang, J.; Huang, Y.; Li, Z.; Zhang, J.; Kuang, H.; Chen, S.; Nie, Z.; Huang, S.; Li, W.; et al. A high-performance free-standing Zn anode for flexible zinc-ion batteries. *Nanoscale* **2021**, *13* (22), 10100−10107.
(51) Zhao, K.; Wang, C.; Yu, Y.; Yan, M.; Wei, Q.; He, P.; Dong, Y.; Zhang, Z.; Wang, X.; Mai, L. Ultrathin surface coating enables stabilized zinc metal anode. *Advanced Materials Interfaces* **2018**, *5* (16), No. 1800848.
(52) Kang, L.; Cui, M.; Jiang, F.; Gao, Y.; Luo, H.; Liu, J.; Liang, W.; Zhi, C. Nanoporous CaCO3 coatings enabled uniform Zn stripping/plating for long-life zinc rechargeable aqueous batteries. *Adv. Energy Mater.* **2018**, *8* (25), No. 1801090.
(53) Li, Z.; Wu, L.; Dong, S.; Xu, T.; Li, S.; An, Y.; Jiang, J.; Zhang, X. Pencil drawing stable interface for reversible and durable aqueous zinc-ion batteries. *Adv. Funct. Mater.* **2021**, *31* (4), No. 2006495.
(54) Liu, C.; Luo, Z.; Deng, W.; Wei, W.; Chen, L.; Pan, A.; Ma, J.; Wang, C.; Zhu, L.; Xie, L.; et al. Liquid Alloy Interlayer for Aqueous Zinc-Ion Battery. *ACS Energy Lett.* **2021**, *6* (2), 675−683.

https://doi.org/10.1021/acsenergylett.4c02191
ACS Energy Lett. 2024, 9, 5421−5433